DOI: 10.13009/EUCASS2023-143
Aerospace Europe Conference 2023 – 10TH EUCASS – 9TH CEAS

Design of unmanned air vehicles with distributed electric propulsion: range improvement and noise emission

Luis Miguel GARCÍA-CUEVAS⋆†, *Jorge GARCÍA-TÍSCAR*⋆, *Pau VARELA*⋆ *and Federico Nahuel RAMÍREZ*⋆
⋆ *CMT–Motores Térmicos, Universitat Politècnica de València*
Camino de Vera s/n, 46022 Valencia, Spain
luiga12@mot.upv.es · jorgarti@mot.upv.es · pavamar@mot.upv.es · fera1@mot.upv.es
†Corresponding author

Abstract

Due to the wide range of Unmanned Aerial Vehicle (UAV) applications, the current fleet will multiply in the coming years.[1] However, this growth in the UAV fleet will inevitably be accompanied by a series of concerns. Mainly, the scientific community[2] is concerned about both polluting and greenhouse gas emissions, as well as noise emissions in the operation of these aircraft in urban environments.[3] In recent years, multiple technologies have been proposed to alleviate these problems, such as electrification or hybridisation,[4] the use of distributed electric propulsion (DEP),[5] or boundary layer ingestion (BLI).[6] Recently, in the research by Tiseira et al.,[7] the combination of these technologies has been presented to design small fixed-wing aircraft weighing up to 25 kg. Those designs achieve up to 16% fuel savings compared to classic configurations based on ICE-powered mono propellers. This reduction in fuel for the same mission opens the door to designing new aircraft that optimise the application of these technologies, thus reducing the associated pollution and noise. The effect on fuel consumption can also be directly translated into other powerplant configurations, such as fuel cell-battery hybrids or direct battery-powered aircraft. In this work, a least absolute shrinkage and selection operator (lasso) method is employed with an aircraft design database to develop tools that can aid the DEP BLI aircraft conceptual and preliminary design. Although the objective of the design procedures is to minimise energy consumption, the final configuration impacts the acoustic signature of the aircraft, which is an important concern during missions such as urban flight or patrol operations. Thus, the impact on noise emissions is also studied.

1. Introduction

The increase in the drone fleet is imminent, according to multiple specialised studies,[8–10] which should not be surprising since, as time goes, there are more applications for these aircraft.

However, fleet growth also brings challenges. Even if only small aircraft are considered, the rise in greenhouse, pollution, and noise emissions can not be despised. That is why research must focus on the application of technologies that allow the reduction of said emissions. In recent years some of these technologies have stood out with surprising results in terms of reducing emissions, highlighting Distributed Electric Propulsion (DEP) and Boundary Layer Ingestion (BLI).

Advances in batteries have facilitated the electrification of aircraft propulsion plants, especially in small aircraft, where the weight of the necessary batteries continues to allow competitive flight.[11] The electrification of the propulsion plant has made it easier to increase the distribution of small electric motors along the wing, which can provide multiple advantages, including aerodynamic efficiency improvements, vectored thrust and reduced noise footprint as can be seen in the research carried out by Moore and Ning,[12] Kim et al.[13] and Ko.[14]

Additionally, the ease of the electric engine setting may provide further improvement if the distribution is employed near the wing trailing edge, where the propulsor can benefit from the boundary layer ingestion. Many investigations point to a decrease in the power required by the propulsion system when BLI is applied through propulsive and aerodynamic efficiency gains as concluded by El-Salamony and Teperin,[6] Lv et al.[15] and Martinez and Smith.[16] Furthermore, It has been proven that the combination of both DEP and BLI technologies in small aircraft is possible, obtaining promising results in reducing polluting and greenhouse emissions, as seen in the research by Serrano et al.[17] and Tiseira et al.[7]

Moreover, as mentioned above, acoustic emissions will be one of the main challenges to be overcome in the imminent expansion of UAVs. The noise generated by a UAV can be up to 50% more annoying than that of a bus.[1,18]

DOI: 10.13009/EUCASS2023-143

For this reason advances are being pushed forward not only to reduce the noise level but also to improve the quality of that noise. In particular, research is being carried out on the interaction between two[19,20] or more[21] propellers and low noise propeller design guidelines are being developed.[22–24] Lastly, the noise emission of full UAVs is also being studied, as in the research by T. Zhang, G.N. Barakos, Furqan et al.[25]

The objective of this work is to present the preliminary results of the design and study of a DEP + BLI configuration, both in terms of performance and consumption reduction. In addition, due to the importance it will have in the acceptability of this type of aircraft, the noise generated by such a configuration will be studied.

This paper is structured as follows: first, a brief introduction to the subject and the state of the art has been provided in this section. Then, in section 2 the design methodology followed and a description of the UAV geometry will be provided. In section 3 the numerical set-ups used in Star-CCM+ (subsection 3.1) and OpenFOAM (subsection 3.3) will be detailed. Next, the main results will be reported and discussed in section 4. Finally, in section 5 the main conclusions will be summarised.

2. Aircraft design

2.1 DEP + BLI design method

Due to the interaction of the propulsion system with the aerodynamic performance of the aircraft, the classic conceptual design methods can not be used directly in DEP + BLI configurations. If the changes in the aerodynamic and propulsive efficiencies and the thrust are not computed early on, it is not possible to optimise some parameters such as the number of propellers, their position, size or pitch. In order to overcome that, a simplified model has been developed by the research team, and described in Dr. Varela's PhD thesis.[26] The model takes into account the following predictors as a function of the results observed in this PhD thesis:

$$C_{\text{L,section}}, C_{\text{D,section}} = f\left(\alpha, \log Re, \frac{1}{J}, \theta, \frac{d}{x}, \frac{h}{d}, \frac{d}{c}\right), \tag{1}$$

$$C_{\text{T,section}}, C_{\text{P,section}} = f\left(\alpha, \frac{1}{\log Re}, J, \theta, \frac{x}{d}, \frac{h}{d}, \frac{c}{d}\right), \tag{2}$$

where α is the angle of attack, Re is the Reynolds number, J is the advance parameter, θ is the geometrical pitch angle of the propeller, d is the propeller diameter, h is the distance between the propeller shaft and the trailing edge, c is the airfoil chord, and x is the distance between propeller shafts.

Using those parameters is possible to compute the expected lift coefficient ($C_{\text{L,section}}$, see Equation 3), drag coefficient ($C_{\text{D,section}}$, see Equation 4), thrust coefficient ($C_{\text{T,section}}$, see Equation 5) and power coefficient ($C_{\text{P,section}}$, see Equation 6) of a wing section with a propeller, as can be seen in Figure 1:

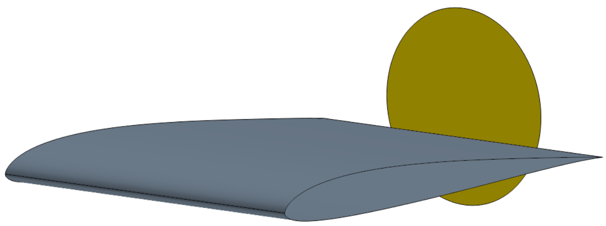

Figure 1: Example of wing section with propeller considered during the development of simulations for the execution of the lasso method. From Dr. Varela's PhD thesis.[26]

$$\begin{aligned} C_{\text{L,section}} = {} & P_1 \cdot \alpha + P_2 \cdot \alpha \cdot \log Re + P_3 \cdot \alpha \frac{d}{J \cdot x} + P_4 \cdot \log Re \cdot \frac{d}{J \cdot x} \\ & + P_5 \cdot \log Re \cdot \frac{d \cdot h}{J \cdot x \cdot c} + P_6 \cdot \frac{d^2 \cdot h}{J^2 \cdot x^2 \cdot c} + P_7 \cdot \frac{h^2}{x^2} + P_8 \cdot \frac{d^4}{c^2 \cdot x^2} + P_9, \end{aligned} \tag{3}$$

DOI: 10.13009/EUCASS2023-143

$$C_{\text{D,section}} = Q_1 \cdot \log Re + Q_2 \cdot \frac{d}{J \cdot x} + Q_3 \cdot \alpha \frac{d}{J \cdot x} + Q_4 \cdot \log re \cdot \theta \cdot \frac{d}{x} + Q_5 \cdot \frac{h \cdot d}{J \cdot x^2} + Q_6 \cdot \frac{d^3}{J \cdot x^2 \cdot c} + Q_7 \cdot \frac{d \cdot h^2}{J \cdot x^2 \cdot c} + Q_8 \cdot \alpha^2 + Q_9 \cdot (\log Re)^2 + Q_{10} \cdot \frac{d^2 \cdot h^2}{J^2 \cdot x^2 \cdot c^2} + Q_{11}, \tag{4}$$

$$C_{\text{T,section}} = R_1 \cdot J + R_2 \cdot \theta + R_3 \cdot J \cdot \frac{h}{d} + R_4 \cdot J^2 + R_5 \cdot \theta^2 + R_6, \tag{5}$$

$$C_{\text{P,section}} = S_1 \cdot \theta + S_2 \cdot \alpha \cdot \frac{x}{d} + S_3 \cdot J \cdot \frac{h}{d} + S_4 \cdot \theta \cdot \frac{c}{d} + S_5 \cdot \frac{x \cdot c}{d^2} + S_6 \cdot J^2 + S_7 \cdot \theta^2 + S_8. \tag{6}$$

The parameters of these equations (P_1 to P_9, Q_1 to Q_{11}, R_1 to R_6 and S_1 to S_8) are fitted against a database of several hundred simulations of sections with different propeller positions, sizes, pitches, distances between propellers, angles of attack and Reynolds numbers. The sampling space was selected using a latin-hypercube-sampling method (LHS),[27] whereas the predictors and coefficients of the correlations were selected and fitted using a least absolute shrinkage and selection operator, commonly known as lasso.[28]

The correlations are then used during the conceptual design phase, modifying the performance of the section of the wing affected by DEP and the performance of the propellers affected by BLI.

2.2 Aircraft description

The geometry used in this study is that of the H-200 prototype, developed within the framework of the HYDRONE project, and can be seen in Figure 2. This UAV is being designed at the Universitat Politècnica de València (UPV) with the aim of developing a platform that allows experimenting with concepts such as distributed propulsion, boundary layer ingestion, or the use of hydrogen fuel cells in aeronautic applications. It is an unmanned aircraft with a wingspan of 2.95 m designed for a maximum take-off mass of 15 kg.

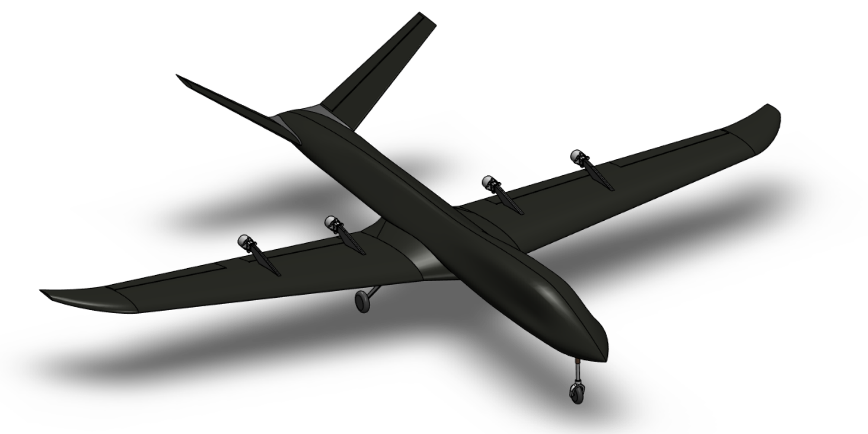

Figure 2: H-200 prototype CAD without the propellers

The aircraft uses distributed electric propulsion over the trailing edge of the wing. A preliminary report describing the design process of the aircraft is available in RiuNet,[29] the public repository of UPV.

Two different geometries have been used for this work. For the first batch of simulations, a realistic geometry has been used, including the landing gear and the channels that are formed in the wing because of the different control surfaces. On the other hand, for the second batch for acoustic results, the geometry has been simplified in order to reduce the number of cells required and to keep the computational cost bounded. Both geometries include the engine pylons on the top of the wing in order to take into account their influence on the flow both over the wing and at the propeller. In all the simulations, the XOAR 9X7 wooden commercial propeller has been employed.

DOI: 10.13009/EUCASS2023-143

3. Methodology

3.1 STAR-CCM+ CFD setup

The first batch of simulations were performed with STAR-CCM+. The STAR-CCM+ simulations comprise a large domain containing half of an aircraft cut by a symmetry plane with two actuator discs modelling both propellers. Downstream the boundary is set at 84 m as a static pressure outlet. At the same time, a free stream speed is imposed on the other boundaries of the domain through a velocity inlet boundary with constant speed, angle of attack components, turbulence intensity, and turbulence length scale. The upstream boundary is set at 24 m, and all the domain has a constant square section of 24 m. The computational domain can be seen in Figure 3.

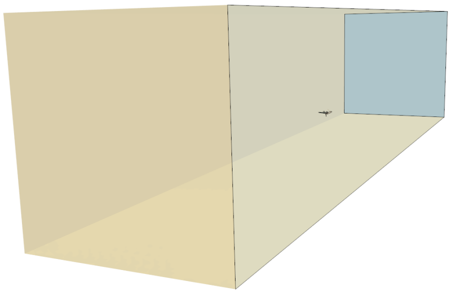

(a) Computational volume

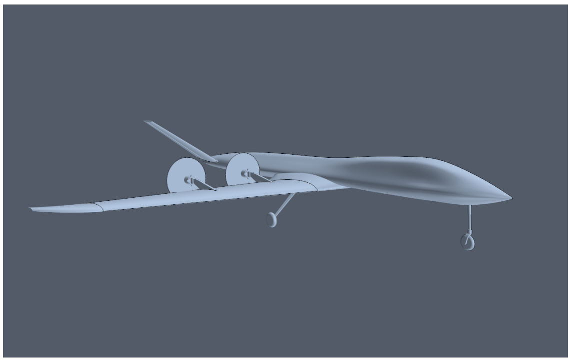

(b) Computational volume detail

Figure 3: STAR-CCM+ computational domain and volume detail.

The size of the domain is proven to be big enough in order not to affect the solution. A non-slip wall condition is imposed in all the aircraft, while the actuator discs are modeled using a blade element method theory (BEMT)[30] actuator disc in a similar way to what was done by Serrano et al.[31] The rotational speed of the actuator disc is imposed through the advance ratio parameter, defined as $J = U/(n \cdot d)$, where U is the flight velocity, n is the propeller rotational speed and d its diameter. The definition is the standard one used for propellers, so the flight velocity is written in $\mathrm{m\,s^{-1}}$, the diameter in m and the rotational speed in Hz.

A Reynolds-Averaged Navier-Stokes (RANS) approach with finite-volume equations have been employed using this software. The Reynolds stress tensor is modeled using the Spalart-Allmaras[32] turbulence model, while the advection and diffusive terms are solved using second-order methods. The flow is always modeled as incompressible since the flow speed and the propeller's rotational speed are considered small. A polyhedral mesh with a minimum edge size of 250 µm and a maximum edge size of 10 mm is employed over the surface of the aircraft, and is shown in Figure 4. Here, a 20-layer prismatic mesh with a geometric growth distribution is applied in a total thickness of 10 mm in order to keep y^+ smaller than 1. Additionally, a prismatic mesh of one layer with the same minimum base size thickness as the polyhedral mesh, is applied on both sides of the actuator disc. This way, it can be ensured that no cells are passing through the actuator disc, which could cause failure in the BEMT model. The total number of cells used in these simulations is 7×10^6 (equivalent to 14×10^6 cells for the full aircraft).

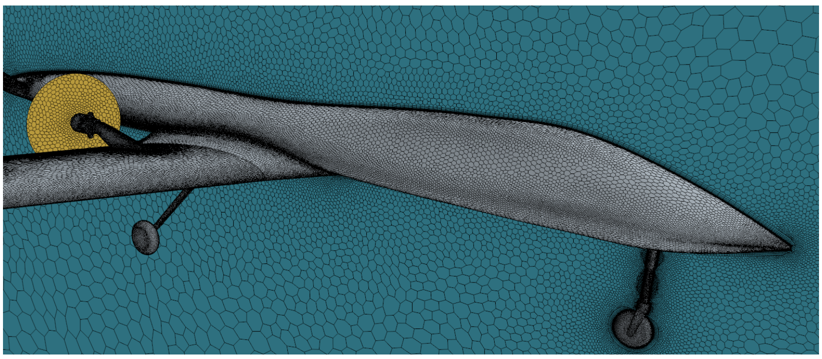

Figure 4: Computational mesh detail employed in STAR-CCM+ simulations

DOI: 10.13009/EUCASS2023-143

Additional simulations of the H200 without propellers and simulations of only the actuator disc were also performed for further comparison.

The simulations were performed at two different airspeeds ($20\,\mathrm{m\,s^{-1}}$ and $22\,\mathrm{m\,s^{-1}}$), for angles of attack between $-2°$ to $10°$ and for values of J between 0.05 and 0.75.

3.2 Steady performance post-processing

After achieving convergence, the following results were computed: the force normal to the incident flow speed due to pressure and shear stress over the surface of the aircraft (lift), the force parallel to the incident flow speed due to pressure and shear stress over the surface of the aircraft (drag), to torque of each of the propellers and the thrust of each of the propellers. The, the non-dimensional lift and drag coefficients were computed, as well as the thrust coefficient and power coefficient for each propeller. Also, the aerodynamic efficiency of the aircraft, the propulsive efficiency of each propeller and the propulsive efficiency of the set of propellers were also computed.

3.3 OpenFOAM CFD setup

OpenFOAM v2112 has been used for the transient simulations applying the sliding mesh methodology. The solver used is rhoPimpleFoam, which is a compressible solver that combines the SIMPLE[33] and PISO[34] algorithms. This approach allows the use of Courant numbers greater than 1 while maintaining the stability of the simulation.

This configuration has been used both to simulate the XOAR 9x7 propeller isolated and to analise the H-200 with the four propellers at a particular operating point. In both cases the simulation has been performed at $20\,\mathrm{m\,s^{-1}}$ and J=0.5.

The simulation of the isolated propeller has been carried out using a spherical computational volume with a diameter 20 times that of the propeller. The computational volume is divided into two zones, one that rotates with the propeller and one that remains stationary, both coupled with an Arbitrary Mesh Interface (AMI).

Regarding the full UAV simulation, its geometry has been simplified, eliminating the landing gear and the channels of the control surfaces. The four propellers were placed in the same position as previously studied, with the four interfaces between the rotating zones and the static mesh defined as AMIs. The rotation of the propellers has been defined in the same direction as for the BEMT simulations, and an offset of 0 degrees has been imposed between them.

The computational volume consists of a hexahedron of $11 \times 6 \times 6$ metres (Figure 5). Several refinement regions have been defined to correctly capture the different phenomena present:

- A $5\,\mathrm{m} \times 3.5\,\mathrm{m} \times 0.8\,\mathrm{m}$ box to capture the wake of the UAV,
- A sphere with a radius of 2.286 m in order to preserve the acoustic waves up to the FW-H surface, and
- A cylinders with a length of 1.14 m and a radius of 0.225 m meters for each propeller wake.

This results in a 25 750 000 cells mesh, with 50 000 faces on the surface of each propeller and 1 385 000 faces at the UAV surface. The first cells at the UAV surface have an edge size of 1.56 mm, while at the surface of the propeller, 3 layers were added to get a cell size of 0.187 mm.

In both simulations a pressure of 101 325 Pa and a velocity of $20\,\mathrm{m\,s^{-1}}$ is set at the boundary of the computational volume, and a no-slip velocity condition and zero gradient pressure condition is set to the UAV and propeller geometries.

As for the numerical configuration, for both set-ups, URANS turbulence modelling has been used, employing the Spalart-Allmaras[32] model with wall functions. Second-order Crank-Nicolson[35] scheme with a blending coefficient of 0.9 for time discretisation. Gauss gradient scheme with a cell-based linear interpolation has been used for the spatial discretisation of the gradient. Lastly, the divergences have been computed using as well the Gauss gradient scheme, but with the first-order upwind scheme[36] for the turbulence and second-order upwind[37] for the rest of the variables.

Finally, the Ffowcs-Williams & Hawkings acoustic analogy has been used to propagate the noise from the CFD computational volume to the desired points. The FW-H Farassat 1A[38] formulation has been applied through the libAcoustic OpenFOAM library.[39,40] Given that it is a low-velocity flow the quadrupole source term has been neglected, thus avoiding volumetric integrations and reducing the computational cost. The FW-H surface used for the isolated propeller is a sphere with a radius six times the diameter of the propeller. For the full UAV simulation, a sphere with a radius of nine times the diameter of the propeller was used.

DOI: 10.13009/EUCASS2023-143

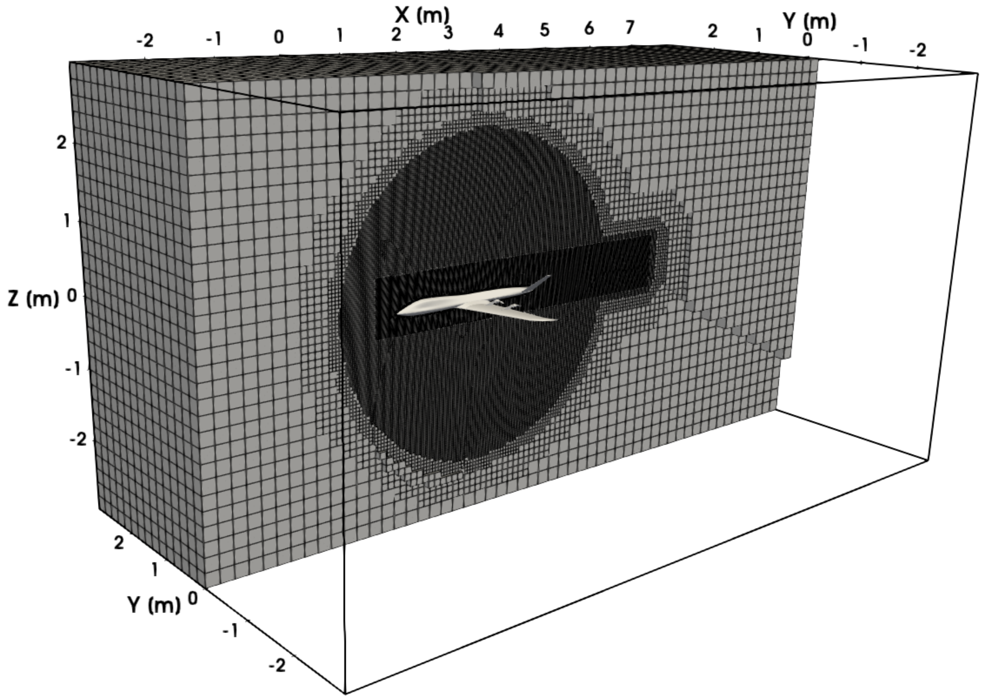

Figure 5: Detail of OpenFOAM computational volume and mesh.

3.4 Acoustic post-processing

Once the transient simulations have converged and sufficient time has been simulated for the flow to fully develop, the FW-H analogy is switched on to perform the acoustic modelling. For this purpose, for the OpenFOAM case, the acoustic signal was recorded at each time-step (25 µs) for at least 0.1 s. This results in a 10 Hz frequency resolution.

Two different metrics have been used to study the acoustic emission. On the one hand, the overall sound pressure level (*OASPL*) is computed using Equation 7, where P_{RMS} is the root mean square of the pressure and P_0 is the reference sound pressure (20 µPa). On the other hand, the pressure signal is used to perform a Welch periodogram[41] using a Blackman window and a 60% overlap. This output is used to compute the sound pressure level spectrum with Equation 8.

$$OASPL = 20 \cdot \log_{10}\left(\frac{P_{\mathrm{RMS}}}{P_0}\right) \tag{7}$$

$$SPL = 10 \cdot \log_{10}\left(\frac{PSD}{P_0^2}\right) \tag{8}$$

4. Results and Discussion

4.1 Performance

With only four propellers over the trailing edge, the DEP and BLI effects in this configuration are limited. Figure 6 shows the thrust coefficient C_T and propulsive efficiency η_p of both the inboard and outboard propellers, as well as the curves for an isolated propeller. The propulsive efficiency peak is moved towards higher advance ratios J, as the average flow speed at the inlet of the propellers is reduced due to the boundary layer ingestion.

Table 1 shows a summary of the results flying at $20\,\mathrm{m\,s^{-1}}$ and $22\,\mathrm{m\,s^{-1}}$ for both the DEP + BLI configuration as well as a clean configuration in which the propellers do not interact with the rest of the aircraft. The results are obtained in straight and level conditions, so the summary of forces applied to the aircraft (lift, drag, thrust and weight) is exactly 0. At both speeds, there is a 4 % improvement in the aerodynamic efficiency, explained by the effect of BLI. The aerodynamic efficiency is the same at $22\,\mathrm{m\,s^{-1}}$, but it is slightly smaller in the DEP + BLI case at $20\,\mathrm{m\,s^{-1}}$. This results in a final improvement in the product of efficiencies of 3 % at $20\,\mathrm{m\,s^{-1}}$ and 4 % at $22\,\mathrm{m\,s^{-1}}$. The efficiency improvement is expected to be even higher against a realistic puller configuration, as the wake of the propellers is expected to increase the aircraft drag for a given lift in that case.

DOI: 10.13009/EUCASS2023-143

Figure 7 shows the results of the product of efficiencies for a range of angles of attack α and values of J. In the figure, the dashed line represents the points in which the lift is equal to the weight of the aircraft, whereas the dotted line represents the points in which the thrust is equal to the aircraft drag. The effect of the BLI can also be seen in these curves: the dashed line is not perfectly straight and vertical, as the propellers provide some extra lift at high rotational speed.

Although non-negligible, the effects are not so impressive as in other works. This is explained by two different reasons. On one hand, the propeller diameter - wing chord ratio is relatively high, so the boundary layer ingestion effects are limited to a somewhat small fraction of the propeller disc. On the other hand, only around half of the wingspan is affected by the propellers, limiting the effects in the aerodynamic efficiency. The propellers are also placed in a relatively low position: as the BLI effect on the propeller is increased and the suction peak is decreased in lower positions against higher positions, smaller improvements in the aerodynamic efficiency and higher increases in propulsive efficiency are produced. A higher position would have reduced the propulsive efficiency with no net clear improvement in aerodynamic efficiency, as a bigger downforce in the stabilisers would have been needed due to the pitch-down moment of the propellers. The number of propellers was limited due to constraints in the availability of the electronic components selected for manufacturing the aircraft: higher efficiencies were expected by reducing their diameter and doubling their number.

Table 1: Performance results

	$20\,\mathrm{m\,s^{-1}}$		$22\,\mathrm{m\,s^{-1}}$	
	Isolated	DEP + BLI	Isolated	DEP + BLI
η_p	0.725	0.752	0.727	0.756
L/D	11.57	11.48	10.52	10.52
$\eta_p \times L/D$	8.39	8.63	7.59	7.92

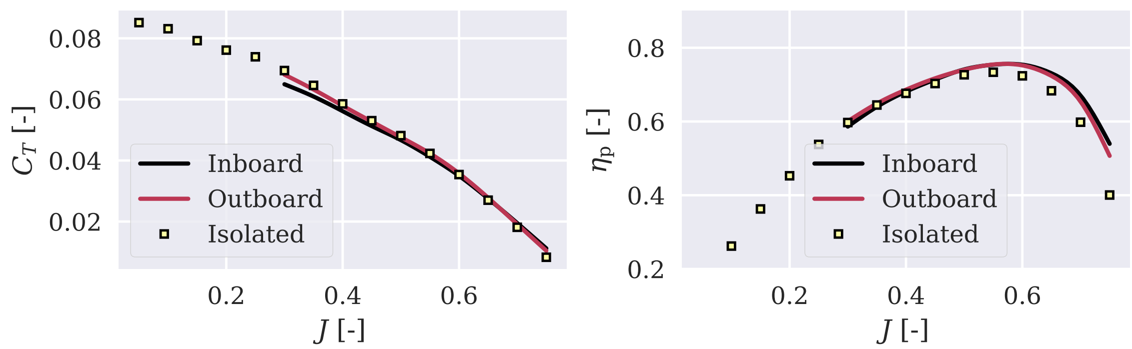

(a) Thrust coefficient

(b) Propulsive efficiency

Figure 6: Propeller results.

4.2 Acoustics

Regarding the OpenFOAM results, when comparing the propulsive efficiency of the isolated propeller with that of the propellers in DEP + BLI configuration, an improvement in propulsive efficiency of 3% and 3.28% are observed at the outboard and inboard propellers respectively. These results are in agreement with the conclusions obtained with STAR-CCM+ using BEMT.

Moving on to the acoustic results, Figure 8 shows the pressure time derivative for the instant 0.3 s. It can be noticed that the main sources of noise are the four propellers. The noise generated by the propeller propagates from its surface, interacting both with the waves generated by the rest of the propellers and with the UAV fuselage. It is also observed that the wake of the propellers does not represent a notable source of noise, or at least URANS modelling is not able to take it into account.

Figure 9 shows the directivity pattern of both, the OASPL and the SPL at the blade passing frequency (350 Hz) of the propellers. The results obtained from both the complete simulation of the UAV with the four propellers, and form aggregating the independent signal of four isolated propellers are shown.

DOI: 10.13009/EUCASS2023-143

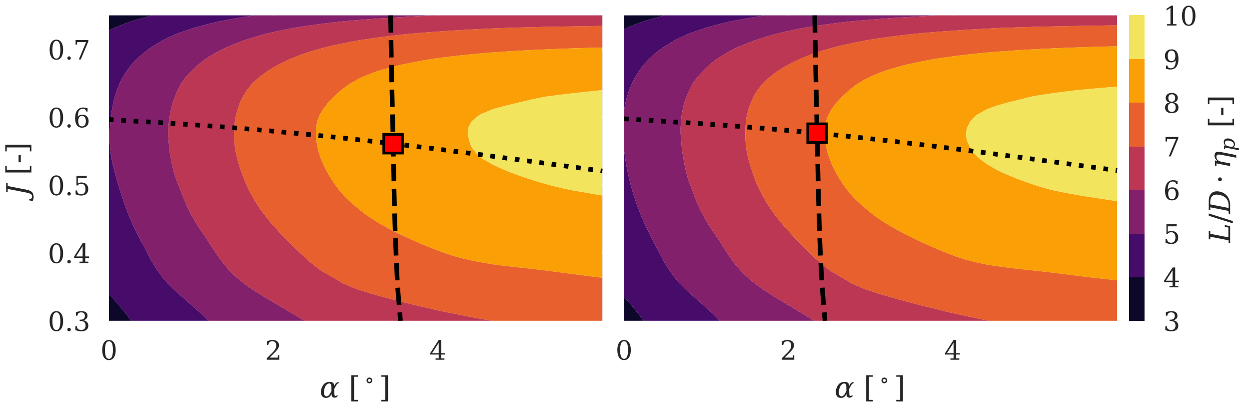

(a) $U = 20\,\mathrm{m\,s^{-1}}$ (b) $U = 22\,\mathrm{m\,s^{-1}}$

Figure 7: DEP + BLI efficiency. The dashed line represents the points in which the lift is equal to the aircraft weight. The dotted line represents the points in which the thrust is equal to the aircraft drag.

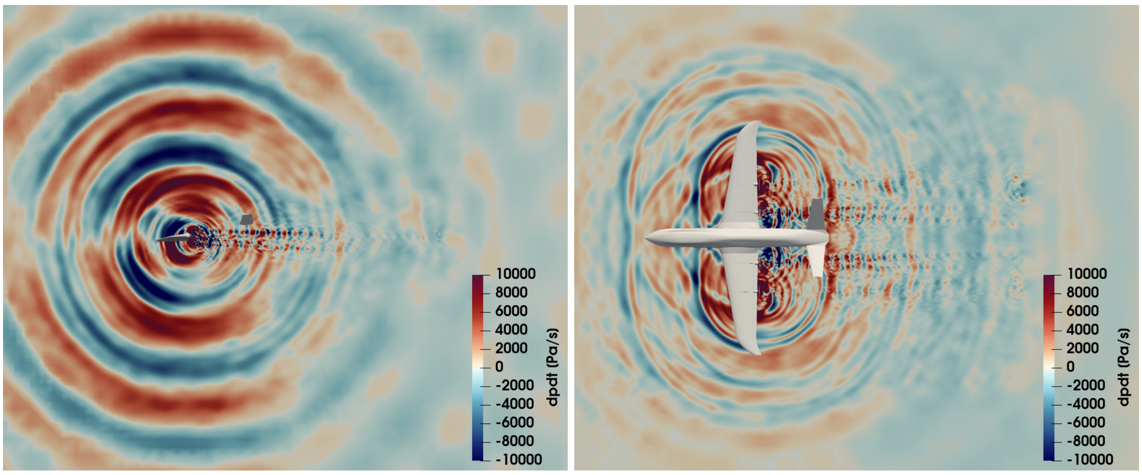

Figure 8: Pressure time derivative at time = 0.3 s.

Analysing the complete UAV results, it can be observed that the directivity is slightly shifted towards the flight direction (180°) and upwards (90°). As for the comparison with the results obtained by the aggregation of the signal of four isolated propellers, it can be noticed that not considering the interactions between propellers and with the airframe (shown in Figure 8) implies an underestimation of the noise generated. The error ranges from 6 dB-7.8 dB in the flight direction and 11 dB-15.65 dB in the vertical direction for the OASPL. As for the SPL at the BPF, it is observed that the error committed increases significantly (up to 23 dB) at the upstream microphone.

Figure 10 shows the frequency spectrum of the sound pressure level at four different positions around the UAV (0°, 90°, 180° and 270° at a radius of 5 m). It is important to note that URANS modelling is being performed, and therefore, turbulence is not being simulated. Consequently, it is expected not to obtain information concerning broadband noise in the frequency spectrum.

It shows the difference between the two approaches. Modelling from 4 isolated propellers allows capturing (although underestimating) the noise at the blade passing frequency and its harmonics. However, the noise generated at half that frequency and its harmonics that appears in the simulation of the full UAV is not observed. This noise is most likely caused by the interaction of the acoustic waves of the propellers with each other and with the pressure differential caused by the wing of the UAV.

It is also important to note that the reason for the large difference at the upstream location in Figure 9 is due to the fact that the 4 independent propeller model has not been able to properly capture the noise generated at the blade passing frequency.

DOI: 10.13009/EUCASS2023-143

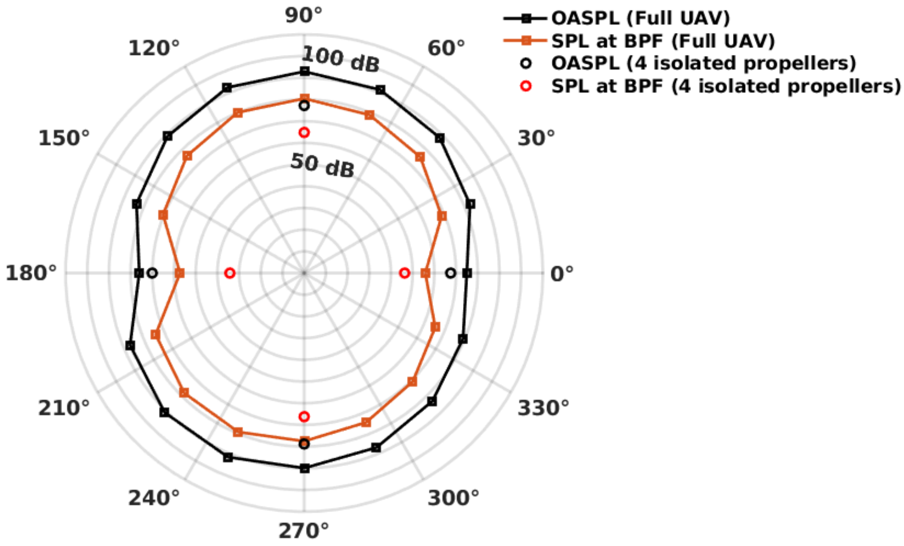

Figure 9: Directivity of OASPL and SPL at BPF at a radius of 5 m of the full UAV (squares), and that calculated from the simulation of 4 isolated propellers disregarding the interaction between them and with the airframe (circles). Flight direction from 0° to 180°.

5. Conclusions

When designing a fixed-wing UAV for long endurance and range missions, distributed electric propulsion configurations are an attractive technological solution: making use of boundary layer ingestion, the overall efficiency of the aircraft can be increased and, thus, the energy consumption can be reduced. Even when a small number of propellers are used, DEP and BLI appear to generate non-negligible improvements in the efficiency of the vehicle. In this work, using 4 relatively big propellers, an increase of 4 % in overall efficiency can be achieved against a case in which the propellers do not interact with the rest of the aircraft. If compared with a case in which the propellers are placed in a puller configuration in front of the trailing edge of the wing, even higher increases in overall efficiency are expected, as the wake of the propulsion system is expected to generate an important penalty in the friction drag over the wing in that case.

Regarding the noise emissions, a first modelling of the noise generated by the DEP + BLI aircraft has been carried out. Acoustic directivity has been studied with two different approaches, proving the importance of the interaction between propellers and the airframe and, therefore, the importance of taking into account the acoustic emissions in the design process. Indeed, the influence of the airframe and the chosen propeller distribution is not only limited to the overall sound pressure level, since peaks at frequencies corresponding to half of the first blade passing frequency and its harmonics also emerge or amplify.

As a summary, the effects of the interaction between the propulsion system and the rest of the aircraft can not be neglected in these configurations. On one hand, and attending only to aerodynamic and propulsive performance parameters, the authors advise to take into account the interaction effects due to the position, size and number of propellers from the very beginning of the conceptual design phase. On the other hand, and although other authors have found improvements in noise emissions when using DEP, BLI may worsen the noise pollution, so mitigation strategies should be implemented.

6. Acknowledgments

This work was partly sponsored by grant TED2021-131087A-I00 *Digital models for the evaluation and reduction of acoustic pollution generated by UAS in urban environments (MODERA)* funded by MCIN/AEI/10.13039/501100011033 and by the European Union NextGenerationEU/PRTR. It was also partially funded by the Agencia Estatal de Investigación of Spain through grant number PID2020-119468RA-I00 by AEI/10.13039/501100011033. The authors gratefully acknowledge the use of the Rigel computing cluster of Universitat Politècnica de València. The authors also want to acknowledge the astounding work of José Domingo Cerdán Torres, Sergio Alexandro Costea Andronache and Joan Albert Such García designing the UAV, as well as the rest of the team of the HYDRONE project.

DOI: 10.13009/EUCASS2023-143

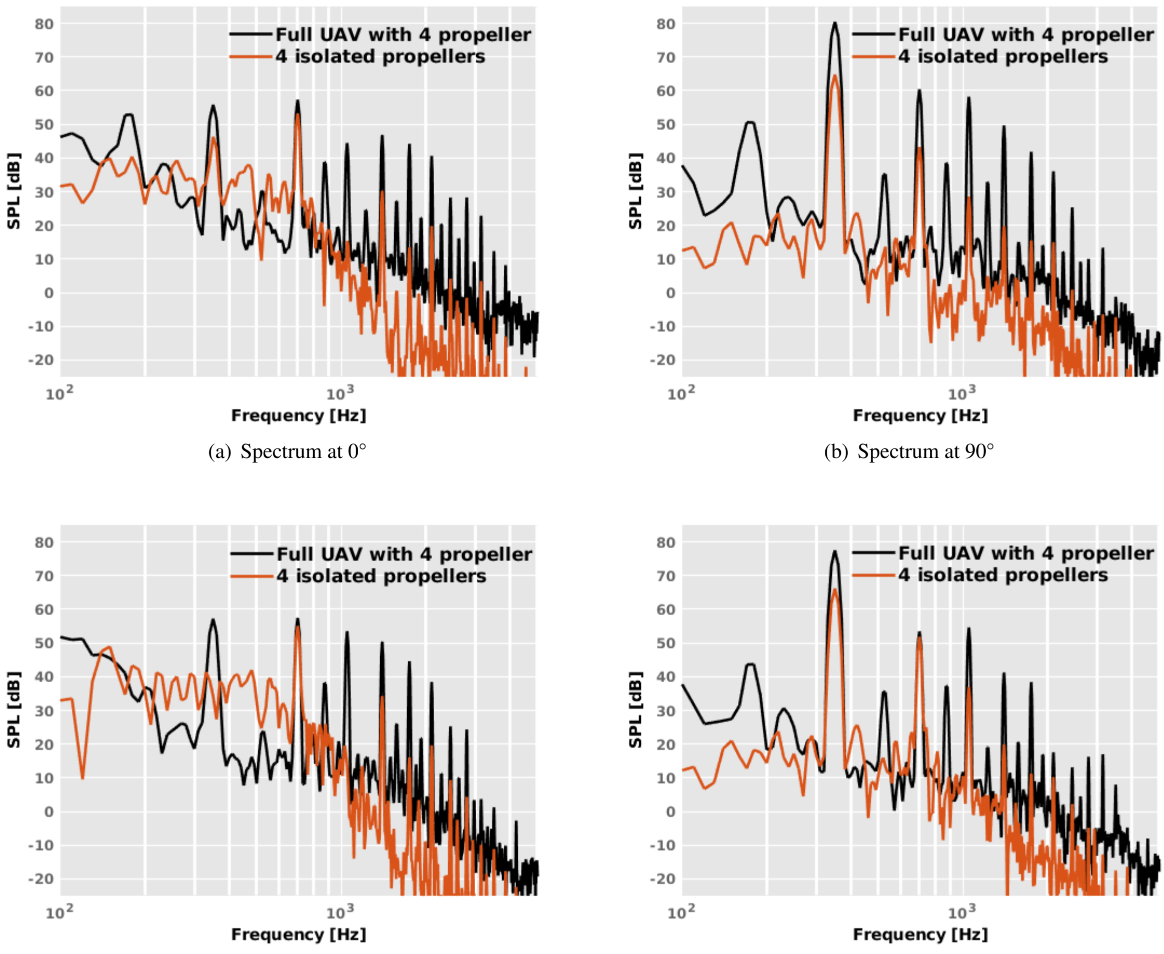

(a) Spectrum at 0°

(b) Spectrum at 90°

(c) Spectrum at 180°

(d) Spectrum at 270°

Figure 10: Frequency spectrum at four positions (0°, 90°, 180° and 270° at a radius of 5 m) calculated for the full UAV and from 4 isolated propellers.

References

[1] McKinsey & Company, Study on the societal acceptance of urban air mobility in europe, EASA report, American Institute of Aeronautics and Astronautics (July 2021).

[2] C. L. Nickol, W. J. Haller, Assessment of the performance potential of advanced subsonic transport concepts for nasa's environmentally responsible aviation project, in: 4th AIAA Aerosp. Sci. Meet., Vol. 0, AIAA, 2016, pp. 1–21.

[3] A. J. Torija, R. H. Self, J. L. T. Lawrence, Psychoacoustic characterisation of a small fixed-pitch quadcopter, INTER-NOISE and NOISE-CON Congress and Conference Proceedings 259 (8) (2019) 1884–1894. URL https://www.ingentaconnect.com/content/ince/incecp/2019/00000259/00000008/art00099

[4] C. Kim, E. Namgoong, S. Lee, T. Kim, H. Kim, Fuel economy optimization for parallel hybrid vehicles with cvt, in: SAE Technical Paper, SAE, 1999. doi:https://doi.org/10.4271/1999-01-1148.

[5] K. Moore, A. Ning, "distributed electric propulsion effects on traditional aircraft through multidisciplinary optimization, in: AIAA Structures, Structural Dynamics, and Materials Conference, AIAA, 2018. doi:0.2514/6.2018-1652.

[6] El-Salamony, Mostafa, L. Teperin, 2d numerical investigation of boundary layer ingestion propulsor on airfoil, 2017. doi:10.13009/EUCASS2017-67.

DOI: 10.13009/EUCASS2023-143

[7] A. O. Tiseira Izaguirre, L. M. García-Cuevas González, P. Quintero Igeño, P. Varela Martínez, Series-hybridisation, distributed electric propulsion and boundary layer ingestion in long-endurance, small remotely piloted aircraft: Fuel consumption improvements, Aerospace Science and Technology 120 (2022) 107227. doi:https://doi.org/10.1016/j.ast.2021.107227.
URL https://www.sciencedirect.com/science/article/pii/S1270963821007379

[8] Single European Sky ATM Research, European Drones Outlook Study, last accessed: 2022-01-12 (2016).
URL https://www.sesarju.eu/sites/default/files/documents/reports/European_Drones_Outlook_Study_2016.pdf

[9] Ministerio de Fomento, Gobierno de España, Plan Estratégico para el desarrollo del sector civil de los drones en España 2018-2021, last accessed: 2023-06-23 (2018).
URL https://www.mitma.gob.es/el-ministerio/planes-estrategicos/drones-espania-2018-2021

[10] A. Amoukteh, J. Janda, J. Vicent, Drones Go to work, Harvard Business Review (2017) 77–94.
URL https://hbr.org/cover-story/2017/05/drones-go-to-work

[11] M. WANG, S. ZHANG, J. DIEPOLDER, F. HOLZAPFEL, Battery package design optimization for small electric aircraft, Chinese Journal of Aeronautics 33 (11) (2020) 2864–2876, sI: Emerging Technologies of Unmanned Aerial Vehicles. doi:https://doi.org/10.1016/j.cja.2020.04.021.
URL https://www.sciencedirect.com/science/article/pii/S1000936120302235

[12] K. R. Moore, A. Ning, Distributed electric propulsion effects on traditional aircraft through multidisciplinary optimization, in: AIAA/ASCE /AHS/ASC Structures, Structural Dynamics, and Materials Conference, AIAA, Kissimmee, FL, USA, 2018. doi:10.2514/6.2018-1652.

[13] H. D. Kim, A. T. Perry, P. J. Ansell, A Review of Distributed Electric Propulsion Concepts for Air Vehicle Technology, in: 2018 AIAA/IEEE Electric Aircraft Technologies Symposium, Cincinnati, Ohio, USA, 2018. doi:10.2514/6.2018-4998.

[14] Y.-Y. A. Ko, The Multidisciplinary Design Optimization of a Distributed Propulsion Blended-Wing-Body Aircraft, Ph.D. thesis, Virginia Tech (2003).
URL https://vtechworks.lib.vt.edu/handle/10919/27257

[15] P. Lv, A. G. Rao, D. Ragni, L. Veldhuis, Performance analysis of wake and boundary-layer ingestion for aircraft design, Journal of Aircraft 53 (5) (2016) 1517–1526. doi:10.2514/1.C033395.

[16] A. Martínez Fernández, H. Smith, Effect of a fuselage boundary layer ingesting propulsor on airframe forces and moments, Aerospace Science and Technology 100 (2020) 105808. doi:10.1016/j.ast.2020.105808.

[17] J. R. Serrano, A. O. Tiseira, L. M. García-Cuevas, P. Varela, Computational study of the propeller position effects in wing-mounted, distributed electric propulsion with boundary layer ingestion in a 25 kg remotely piloted aircraft, Drones 5 (3) (2021). doi:10.3390/drones5030056.

[18] A. Christian, R. Cabell, Initial investigation into the psychoacoustic properties of small unmanned aerial system noise, 2017. doi:10.2514/6.2017-4051.

[19] H. Lee, Lee, Numerical prediction of aerodynamic noise radiated from a propeller of unmanned aerial vehicles.

[20] H. Bu, H. Wu, C. Bertin, Y. Fang, S. Zhong, Aerodynamic and acoustic measurements of dual small-scale propellers, Journal of Sound and Vibration 511 (10 2021). doi:10.1016/j.jsv.2021.116330.

[21] B. Smith, F. Gandhi, R. Chair, R. Niemiec, A comparison of multicopter noise characteristics with increasing number of rotors (2020).

[22] P. S. Doijode, S. Hickel, T. van Terwisga, K. Visser, A machine learning approach for propeller design and optimization: Part ii, Applied Ocean Research 124 (7 2022). doi:10.1016/j.apor.2022.103174.

[23] A machine learning approach for propeller design and optimization: Part i, Applied Ocean Research 124 (7 2022). doi:10.1016/j.apor.2022.103178.

DOI: 10.13009/EUCASS2023-143

[24] M. Ghoreyshi, P. Aref, C. F. Wisniewski, J. Seidel, K. W. V. Treuren, Computational investigation of quiet propeller designs for small unmanned aerial vehicles, Aerospace Science and Technology 138 (2023) 108351. doi:10.1016/j.ast.2023.108351.
URL https://linkinghub.elsevier.com/retrieve/pii/S1270963823002481

[25] T. Zhang, G. N. Barakos, Furqan, M. Foster, High-fidelity aerodynamic and acoustic design and analysis of a heavy-lift evtol, Aerospace Science and Technology (2023) 108307doi:10.1016/j.ast.2023.108307.
URL https://linkinghub.elsevier.com/retrieve/pii/S1270963823002043

[26] P. Varela Martínez, On the analysis and design of series hybrid distributed electric propulsion with boundary layer ingestion of remotely piloted aircraft, Ph.D. thesis, Universitat Politècnica de València (2023). doi:10.4995/Thesis/10251/192805.

[27] M. D. McKay, R. J. Beckman, W. J. Conover, A comparison of three methods for selecting values of input variables in the analysis of output from a computer code, Technometrics 42 (1) (2000) 55–61. doi:10.1080/00401706.2000.10485979.

[28] R. Tibshirani, Regression shrinkage and selection via the lasso, Journal of the Royal Statistical Society. Series B (Methodological) 58 (1) (1996) 267–288.
URL http://www.jstor.org/stable/2346178

[29] S. A. Costea Andronache, J. D. Cerdán Torres, J. A. Such García, L. M. García-Cuevas González, S. García-Nieto Rodríguez, Diseño conceptual proyecto h200, Tech. rep., Universitat Politècnica de València (2023).
URL http://hdl.handle.net/10251/194445

[30] R. Rajagopalan, S. R. Mathur, Three dimensional analysis of a rotor in forward flight, in: 20th Fluid Dynamics, Plasma Dynamics and Lasers Conference, 1989. doi:10.2514/6.1989-1815.

[31] J. R. Serrano, L. M. García-Cuevas, P. Bares, P. Varela, Propeller position effects over the pressure and friction coefficients over the wing of an uav with distributed electric propulsion: A proper orthogonal decomposition analysis, Drones 6 (2) (2022). doi:10.3390/drones6020038.
URL https://www.mdpi.com/2504-446X/6/2/38

[32] P. Spalart, S. Allmaras, A one-equation turbulence model for aerodynamic flows, AIAA 439 (01 1992). doi:10.2514/6.1992-439.

[33] L. S. Caretto, A. D. Gosman, S. V. Patankar, D. B. Spalding, Two calculation procedures for steady, three-dimensional flows with recirculation, in: H. Cabannes, R. Temam (Eds.), Proceedings of the Third International Conference on Numerical Methods in Fluid Mechanics, Springer Berlin Heidelberg, Berlin, Heidelberg, 1973, pp. 60–68.

[34] R. Issa, Solution of the implicitly discretised fluid flow equations by operator-splitting, Journal of Computational Physics 62 (1) (1986) 40–65. doi:https://doi.org/10.1016/0021-9991(86)90099-9.

[35] J. Crank, P. Nicolson, A practical method for numerical evaluation of solutions of partial differential equations of the heat-conduction type, Mathematical Proceedings of the Cambridge Philosophical Society 43 (1) (1947) 50–67. doi:10.1017/S0305004100023197.

[36] D. B. Spalding, A novel finite difference formulation for differential expressions involving both first and second derivatives, International Journal for Numerical Methods in Engineering 4 (4) (1972) 551–559. doi:https://doi.org/10.1002/nme.1620040409.

[37] R. F. Warming, R. M. Beam, Upwind second-order difference schemes and applications in aerodynamic flows, AIAA Journal 14 (9) (1976) 1241–1249. doi:10.2514/3.61457.

[38] K. S. Brentner, F. Farassat, Analytical comparison of the acoustic analogy and kirchhoff formulation for moving surfaces, AIAA Journal 36 (8) (1998) 1379–1386. doi:10.2514/2.558.

[39] A. Epikhin, I. Evdokimov, M. Kraposhin, M. Kalugin, S. Strijhak, Development of a dynamic library for computational aeroacoustics applications using the openfoam open source package, Procedia Computer Science 66 (2015) 150–157, 4th International Young Scientist Conference on Computational Science. doi:https://doi.org/10.1016/j.procs.2015.11.018.
URL https://www.sciencedirect.com/science/article/pii/S1877050915033670

DOI: 10.13009/EUCASS2023-143

[40] A. Epikhin, Validation of the developed open-source library for far-field noise prediction, in: Annual Congress of the International Institute of Acoustics and Vibration, 2021. doi:10.5281/zenodo.5906668.

[41] P. D. Welch, The use of fast fourier transform for the estimation of power spectra: A method based on time averaging over short, modified periodograms, IEEE Transactions on Audio and Electroacoustics 15 (1967) 70–73. doi:10.1109/TAU.1967.1161901.